



ARTICLE

Nanofibrillation of Bacterial Cellulose Using High-Pressure Homogenization and Its Films Characteristics

Heru Suryanto^{1,2,*}, Muhamad Muhajir¹, Bili Darnanto Susilo¹, Yanuar Rohmat Aji Pradana¹, Husni Wahyu Wijaya^{2,3}, Abu Saad Ansari⁴ and Uun Yanuhar⁵

¹Department of Mechanical Engineering, Faculty of Engineering, Universitas Negeri Malang, Malang, 65145, Indonesia

²Centre of Advanced Materials for Renewable Energy, Universitas Negeri Malang, Malang, 65145, Indonesia

³Department of Chemistry, Faculty of Mathematics and Natural Sciences, Universitas Negeri Malang, Malang, 65145, Indonesia

⁴Department of Chemical Engineering, Hongik University, Seoul, 04066, Korea

⁵Biotechnology and Waters Sciences Laboratory, Faculty of Fisheries and Marine Science, University of Brawijaya, Malang, 65145, Indonesia

*Corresponding Author: Heru Suryanto. Email: heru.suryanto.ft@um.ac.id

Received: 08 December 2020 Accepted: 01 March 2021

ABSTRACT

The microstructure of bacterial cellulose nanofibers (BCNs) film affects its characteristic. One of several means to engineer the microstructure is by changing the BCNs size and fiber distribution through a high-pressure homogenizer (HPH) process. This research aimed to find out the effects of repetition cycles on HPH process towards BCNs film characteristics. To prepare BCNs films, a pellicle from the fermentation of pineapple peels waste with *Acetobacter xylinum* (*A. xylinum*) was extracted, followed by crushing the pellicle with a high-speed blender, thereafter, homogenized using HPH at 150 bar pressure with variations of 5, 10, 15, and 20 cycles. The BCNs films were then formed through the casting process and drying in the oven at 60°C for 8 h followed by structural, morphological, and optical properties investigation using X-ray diffraction (XRD), scanning electron microscopy (SEM) and Fourier transform infrared (FTIR) spectrometer along with BCNs films porosity, tensile and roughness test. The research showed that the effect of HPH cycle on BCNs resulted in the highest film tensile strength by 109.15 MPa with the lowest surface roughness (Ra) of $0.93 \pm 0.10 \mu\text{m}$ at 10 cycles. The HPH process is effective in controlling BCNs film porosity level. The HPH cycles influence the crystalline index and crystallite size, slightly.

KEYWORDS

Bacterial cellulose; cellulose film; high-pressure homogenizer; nanofibers; pineapple peels

1 Introduction

Globally, about 10^{10} – 10^{11} tons of cellulose per year is extracted from plants or plant wastes [1]. Conventional, plant-based cellulose fiber contains polysaccharides, e.g., hemicellulose and lignin, which reduces the cellulose fiber strength [2]. To overcome this issue, the plant-based cellulose fiber needs more extended and diverse nanocellulose extractions, which, will results in costs enhancement due to assorted chemical components. On the other hand, plant-based cellulose extraction requires a huge number of plants, thus lead to forest encroachment and global warming. Hence, an alternate source of cellulose is



needed. The bacterial fermentation process is another prominent way to extract cellulose. Bacterial cellulose nanofibers (BCNs) production is known using coconut water as a source material [3]. Further, BCNs has successfully produced by the *Gluconobacter xylinum* through a static culture method using the pineapple peels extract medium [4]. Indonesia is known to be the third biggest exporter of the processed pineapples in the world, with the pineapples production capacity of 200,000 tons per year [5]. Thus, it is the great opportunity in developing pineapple peels waste as carbon and nitrogen source for BCNs production.

BCNs, as an environmental friendly polymer resource and substitute to plant-based cellulose, is gaining attention from the world [6]. Due to BCNs biological adaptation capability. Owing to their physical and chemical properties such as high purity, well crystalline, good polymerization level, high absorbance, large water holding capacity, and high tensile strength, etc. BCNs are applied in food industry, medicines, cosmetics, acoustic diaphragm, and papermaking [7,8]. However, there is still a lot of scopes to expand further BCNs applications in various material technology sectors by engineering their properties. Diverse technological approaches are being developed to increase BCNs colloidal suspension property and fiber dispersion [9]. The production of nano-fibrillar BCNs uses a combination of mechanical, chemical, enzymatic, and chemical pre-treatments. The BCNs characteristics not only depends on the base material, but also, disintegration process [10], and treatment method [11]. Some mechanical methods to produce cellulose nanofiber are cryocrushing [12], grinding [13], High-Pressure Homogenizer (HPH) [14], and micro fluidization [15]. The enzymatic method, in combination with the shear mechanic, and HPH leads to cellulose fibrillation to nanometer dimension [16].

The HPH encourages traditional non-thermal process for emulsion stabilization and increasing texture, taste, viscosity, and color uniformity in food industries [17]. The HPH had been applied for micro-fibrillation cellulose suspension treatment in the cellulose [18,19], sugarcane bagasse, and pulp [20]. It is reported that, HPH process had applied in cellulose nanofiber isolation for decreasing the nanofiber diameter from 117 to 67 nm [21,22]. Further, ease of scaling up and operating continuously are the advantages of HPH process. The homogenizer clogging problem which is occurred due to the higher diameter of the fiber can be suppress either by increasing pressure or number of cycles in HPH process. The HPH with increasing pressure from 20 to 60 MPa at constant cycles results in the reduction of cellulose nanofiber diameter, from 94 to 60 nm [7].

The cavitation mechanism, turbulence, shearing, friction, heat, compression, velocity, and fast pressure drop initiates the HPH process [9]. The HPH process is organic solvent-free with high efficiency. Using HPH repeatedly with pressure treatment, one can generate a high fibrillation degree and high cellulose nanofibers (CNFs) [23,24]. The HPH lead to improvement in entanglement due to nano formation in the connected network structure [25]. Several groups used different characterization techniques to investigate the change in BCNs properties. HPH process on BCNs reduces dimension from microscale to nanoscale through crushing force (material particle impact strength), shear stress (material particles interaction in a space), and cavitation (extreme velocity change in the material) [22]. Microstructure information is required in the engineering of the BCNs film formation to find its structural connection towards mechanical properties and parameter in water absorbance, water release, and expansion. Therefore, this study aimed to analyze the effect of HPH cycles on BCNs film characteristics produced using a pineapple peels extract.

2 Experimental

2.1 Materials

The synthesis of BCNs used locally isolate bacteria from *Acetobacter xylinum* species, provided from Microbiology Laboratory, Universitas Negeri Malang, East Java, Indonesia. The chemical sodium hydroxide (purity 98%), acetic acid/CH₃COOH (purity 99%), and ammonium sulfate/(NH₄)₂SO₄ (purity 99%) were purchased from Sigma-Aldrich (Singapore). Pineapple peel waste was obtained from a pineapple plantation at the district of Blitar, East Java, Indonesia.

2.2 Preparation of BCNs film

Initially, the pineapple peels waste (1 kg) were cleaned, blended, pressed, and filtered to get the pineapple peel juice. Thereafter the pineapple peel juice was sterilized. 10% (wt/v) sugar, and 0.5% (v/v) ammonium sulphate (Sigma-Aldrich, Singapore) was added to pineapple peel juice, and the acidity of this culture medium was adjusted to a pH of 4.5 using acetic acid solution (Sigma-Aldrich, Singapore). *A. xylinum* inoculums 20% (v/v) were mixed into the medium of culture then it is fermented for ten days at 30°C. The bacterial cellulose fibers were synthesized in the form of pellicles and floated on the surface of the culture medium. The pellicles were taken and rinsed using distilled water for removing the residual medium and the other impurity. Additionally, pellicles were soaked in 1.0% NaOH solution (Sigma-Aldrich, Singapore) for 24 h then extensively rinsed with distilled water at ambient temperature until the pH of water become neutral. The purified cleaned wet pellicles were cut into smaller sizes and crushed using a high-speed blender (Fomac, ICH-DS7 model, China) at 26000 rpm for five minutes. The resulted suspension was diluted 0.5% (wt/v) by distilled water before homogenization. The suspension homogenization was carried out using HPH equipment (Berkley Scientific, AH-100D model, China) with 5, 10, 15, and 20 cycles at 150 bar pressure. The homogenized samples were poured into a glass mold (17 cm × 12.5 cm) and dried in the oven (Kirin, KBO-250RA model, Indonesia) for eight hours at 70°C. The dried samples were put inside a clipped plastic and stored in the desiccator with 58% humidity at 25°C.

2.3 Characterization

Morphology Analysis. The surface morphology analysis of BCNs films was carried out by FEI, Inspect-S50 scanning electron microscope (Japan) with 30.00 kV operating voltage. Prior to morphology analysis, a thin gold layer of thickness 10 nm was coated on the BCNs films using SC7-620 Emitech sputter coater (UK). The diameter of BCNs film was the average and deviation standard measured by software of ImageJ 1.52a with diameter measurement of 25 times at the SEM photograph. Deviation standard was calculated using statistics function in MS.Excel program.

Structure Analysis. The structural characterization of BCNs film was examined using PAN analytical X'Pert Pro X-ray diffractometer (USA) in the range of $2\theta = 10\text{--}50^\circ$ with $\text{CuK}\alpha$ radiation ($\lambda = 1.54 \text{ \AA}$) at 30 mA and 40 kV. Crystalline index (CrI) is measured using the Segal formula (Eq. (1)) [26], while, the crystallite size was determined using the Scherrer formula (Eq. (2)) [22].

$$\text{CrI}(\%) = \frac{I_{002} - I_{\text{non-cr}}}{I_{002}} 100\% \quad (1)$$

where: CrI represents a crystalline index, I_{002} is maximum peak diffraction at the crystalline plane (002) ($2\theta = 22\text{--}23^\circ$), and $I_{\text{non-cr}}$ is the lowest intensity value for amorphous films (the valley curve from 18° to 20°).

$$\text{Crystallite Size} = \frac{k \lambda}{W \cos \theta} \quad (2)$$

where: $k = 0.89$ is the shape factor (Scherrer's constant), W is the full width half maximum (FWHM) in radian, θ is the Bragg angle, and λ is X-ray radiation wavelength (1.54 Å).

FTIR Analysis. Identification of the functional groups in BCNs was carried out using the Shimadzu IR Prestige-21 Fourier transform infrared (FTIR) spectrometer (Japan). For FTIR measurement, 0.1 mg BCNs was mixed with 1 mg potassium bromide (KBr) powder (high-purity infrared-grade, Sigma-Aldrich, Singapore) and pressed into a pellet. The FTIR spectrum were recorded in the range of 4000 to 400 cm^{-1} with a resolution of 4 cm^{-1} .

Thickness and Surface Roughness Analysis. Both HPH and non-HPH BCNs films thickness at five different areas (15 cm × 20 cm) were measured after drying using a digital micrometer (0.0001 mm resolution, Mitutoyo Co, Japan). For roughness test, we followed the previously published method [27].

The BCNs film surface was analyzed by a portable surface tester (Surftest SJ-301 type, Mitutoyo Co, Japan) with 0.75 mN gauge precision, 0.8 mm λ_c profile filter, average maximum height (Rz), roughness average (Ra), and 4 mm of total length. The roughness measurement rate was 200.0 $\mu\text{m}/\text{cm}$ in a horizontal direction and 5.0 $\mu\text{m}/\text{cm}$ in a vertical direction.

Porosity Analysis. Surface's porosity before and after homogenization process was analyzed by soaking BCNs films in water for four hours at 25°C. Surface porosity was measured using the Eq. (3) [28].

$$\text{Porosity} = \frac{(W_w - W_d)}{(d A D)} \cdot 100\% \quad (3)$$

where: W_w is wet BCNs film weight (g), W_d is dry BCNs film weight (g), d is pure water density at room temperature (1 g/cm^3), D is BCNs film thickness, and A is the surface measurement area (4 cm^2).

Mechanical Properties. The mechanical property, elastic modulus and tensile strength were observed using a tensile tester (Techno Lab., Indonesia) with tension rate of 0.025 $\text{mm}\cdot\text{s}^{-1}$ and maximum load of 50 N. Tensile test of BCNs film was performed ten times with sample dimension referred to ASTM D638-V standard.

3 Results and Discussion

3.1 Morphology of BCNs Film

Fig. 1 shows the morphology of BCNs film before HPH process and after HPH process with various cycles. Clearly, there is a decrease in fiber diameter after HPH process compared to before HPH process (Tab. 1). Precisely, the HPH treatment implication reduces fiber diameter from 61.7 ± 36.98 nm to 46.38 ± 17.18 nm. Further, after HPH process rendered BCNs film becomes more homogenous due to the mechanical process during HPH such as centrifugal extrusion, hydraulic shear, liquid layer friction, and collision between particles.

We observed less reduction in fiber diameter for lower HPH cycles compared to high HPH cycles. The fiber diameter decreases from 53 to 46 nm as HPH cycles increase from 5 to 20. With increasing HPH cycles, BCNs, gradually split from its cellulose fiber and hydrogen bonds into nanofibril. Thus, HPH process with cycle variations changed microfibrils structure into the different nanofibrils structure. Additional passes contribute to the increase of surface area on the cellulose fibrils. This result was in accordance with other results research that shows after 10 passes, the diameter of most cellulose fibrils was in the range from 28 to 100 nm [29,30].

SEM of BCNs represented considerably interesting phenomena about the morphology. Fig. 1a shows BCNs film without HPH treatment. It shows porous film with many debris from culture residue. With mechanical treatment consisting of 5 and 10 passes through the HPH, there were some indications of fibrillation, the culture residue have reduce with smoother film obtained (Figs. 1b, 1c). However, with treatment of 15 to 20 passes through the HPH, these film tend to solid film with little porosity (Figs. 1d, 1e). This is caused of the expected high density of hydroxyl groups at the increased surface area make strongly interact and tend to agglomerate.

3.2 XRD Analysis

Fig. 2 depicts XRD spectra of BCNs films. The content of amorphous and crystalline constituents of BCNs films were examined from these spectra. Three characteristic diffraction peaks in all samples corresponding to crystalline plane of $1\bar{1}0$, 110, and 002 [31] of cellulose were observed at 2θ value of 14.3° , 16.4° , and 22.4° , respectively. The highest intensity peak at 22.4° represents the cellulose type I [32,33].

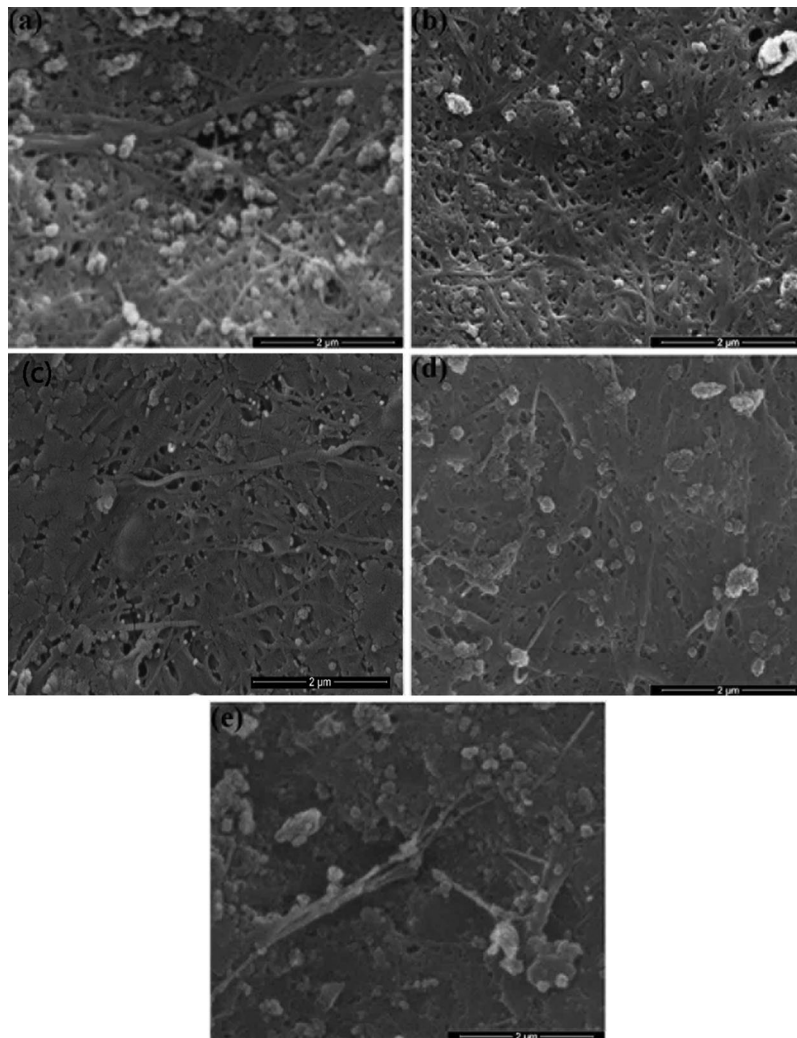


Figure 1: Surface morphology of BCNs film: (a) Non-HPH; (b) 5 cycles, (c) 10 cycles, (d) 15 cycles, and (e) 20 cycles

Table 1: Fiber diameter of BCNs film after HPH process with various cycles process

Samples	Control	5 cycles	10 cycles	15 cycles	20 cycles
Fiber diameter (nm)	61.7 ± 36.98	53.24 ± 27.05	49.82 ± 19.32	47.2 ± 15.34	46.38 ± 17.18

Generally, such XRD spectra having aforementioned peaks refer to cellulose Ia of BCNs film generated from pineapple peels extract. A similar result has reported earlier using sugarcane molasses medium [34] and from agro-industrial waste [35]. Clearly, the HPH process and variation in the number of cycles of HPH process reduce on the crystallite size, and CrI. However, there is no crystal form transformation as no new peak was detected in the diffraction spectra of BCNs after HPH process. With increase in HPH cycles, CrI decreased from 83% (control) to 82%, 81%, 76%, and 74% at 5, 10, 15, 20 cycles, respectively. Also, crystallite size was found to decrease from 29.2 nm (control) to 28.9 nm, 26.9 nm, 23.6 nm and 22.3 nm at 5, 10, 15, 20 cycles, respectively, as shown in Tab. 2. The reduction of crystallinity with increasing cycles might be due to surface crystallites peeling off under multiple shear

and impact forces. Eyholzer et al. [36] reported that the mechanical disintegration and carboxymethylation leads to a decline in the crystallinity of nanofibers [36].

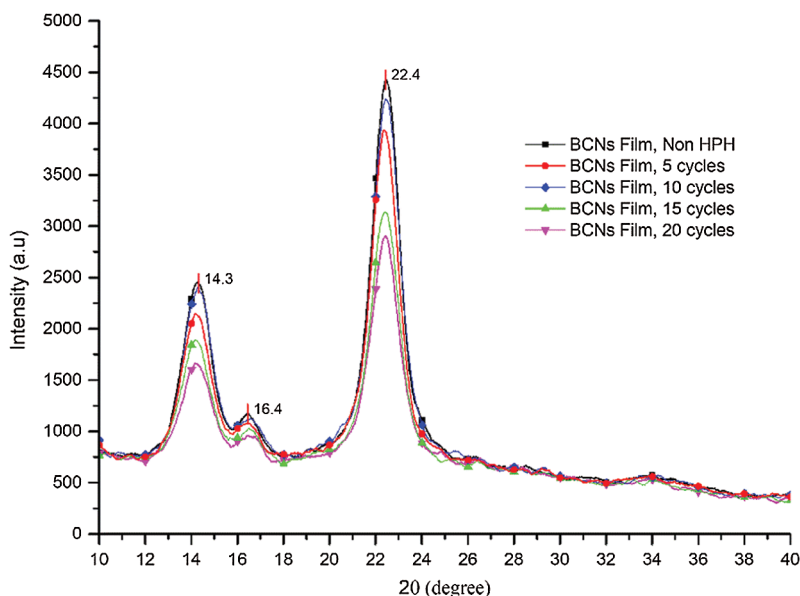


Figure 2: XRD analysis of BCNs film (a) Non-HPH, (b) 5 cycles, (c) 10 cycles, (d) 15 cycles, and (e) 20 cycles

Table 2: Crystalline index and crystallite size of BCNs film after HPH with various cycles process

Samples	Control	5 cycles	10 cycles	15 cycles	20 cycles
Crystallinity index (%)	83	82	81	76	74
Crystallite size (nm)	29.8	28.9	26.9	23.6	22.3

3.3 FTIR Analysis

The effect of homogenization treatment on BCNs film chemical structure is shown in Fig. 3. The transmittance signal at $\sim 3423\text{ cm}^{-1}$ appeared due to OH group stretching vibration from cellulose I type. The signals due to CH_2 stretching and bending mode observed at ~ 2901 and $\sim 1423\text{ cm}^{-1}$ respectively. Signal at $\sim 2137\text{ cm}^{-1}$ is due to $\text{C}\equiv\text{C}$ group stretching vibration of alkynes. While $\sim 1649\text{ cm}^{-1}$ depict the O-H signal of absorbed water and $\sim 678\text{ cm}^{-1}$ for O-H out of plane bending vibration. The signal at $\sim 1173\text{ cm}^{-1}$ was assigned to C-O bending vibration.

Further, peak at $\sim 1127\text{ cm}^{-1}$ is due to C-O-C asymmetric stretching from β -glycosidic link, 1091 cm^{-1} correspond to C-O-H stretching vibration of the sugar ring, and $\sim 899\text{ cm}^{-1}$ for C-O-C β -glycosidic linkages between glucose units and cellulose type I [37]. Characteristic signal found at 899 cm^{-1} and $\sim 1423\text{ cm}^{-1}$ confirms the samples as cellulose type I [22]. The bands of all samples in FTIR spectra are almost similar indicating no changes in the cellulose type. Additionally, the peak intensity at $3000\text{-}3500\text{ cm}^{-1}$ corresponds to hydroxyl group stretching vibration is might be an effect of interference in cellulose tissue and change in defibrillation into nanofibrils during HPH cycles. The FTIR results suggest that, though, there is a slight reduction in the transmittance peak intensity, but, the HPH process does not affect the BCNs chemical group.

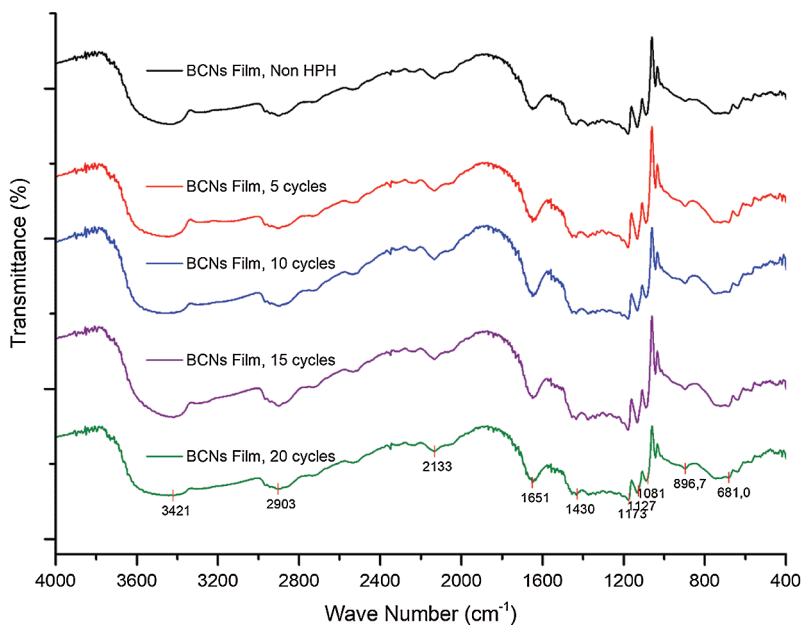


Figure 3: FTIR analysis of BCNs film (a) Non-HPH, (b) 5 cycles, (c) 10 cycles, (d) 15 cycles, and (e) 20 cycles

3.4 Surface Roughness and Thickness Analysis

The comparative roughness profile with different HPH process cycles in the forming of BCNs film is shown in Fig. 4. It can be observed that BCNs film before HPH process has a different roughness and after HPH treatment for 10 cycles BCNs film become smooth. The average roughness (R_a), height of average roughness (R_z), root mean square roughness (R_q), and thickness (t) of BCNs film with different HPH process cycles are given in Tab. 3.

The R_a for the BCNs before HPH and after 5 cycles HPH was found to be similar. Though decrease in R_a from 1.11 ± 0.06 to 0.93 ± 0.10 μm was observed with increase in HPH cycles from 5 to 10, but R_a increase back with increase in further HPH cycles. The BCNs film prepared after 10 HPH cycles is smoother compared to all. Like R_a , similar feature in R_z is observed. R_z decreases from 6.30 ± 0.32 to 5.43 ± 0.48 μm after HPH 10 cycle compared to 0 cycles, and then it increases back with increase in further HPH cycles. R_q also shows similar trend like R_a and R_z , i.e., R_q decrease after HPH and minimum R_q value was observed for 10 cycles HPH (1.15 ± 0.11 μm), but increases back for 15 and 20 cycles of HPH.

BCNs film thickness was found to decreased from 0.042 to 0.029 μm for 5 cycles HPH process compared to 0 cycle HPH. Increase in HPH cycles results in further decrease in BCNs film thickness. Though BCNs film with 20 HPH cycles depict lowest thickness, but, film prepared at 15 cycles HPH shows the lowest standard deviation (0.0016 μm).

Briefly, the HPH process reduces the fiber diameter of different BCNs suspension (Tab. 1). The properties of BCNs films obtained from suspension largely depend on the dispersion and size of BCNs in the suspension. The prepared BCNs films showed different roughness due to the randomly arranged BCNs film structure, twists, and bundles (Fig. 1), which is caused by rearrangement, interlacing of elementary fibrils and self-assembly of the concentrated cellulose through strong hydrogen bonds, and van der Waals forces, thus result in different morphology [38,39]. Thereby BCNs film thickness has inverse relation with HPH cycles, i.e., film thickness decreases with increase in HPH cycles and vice-versa.

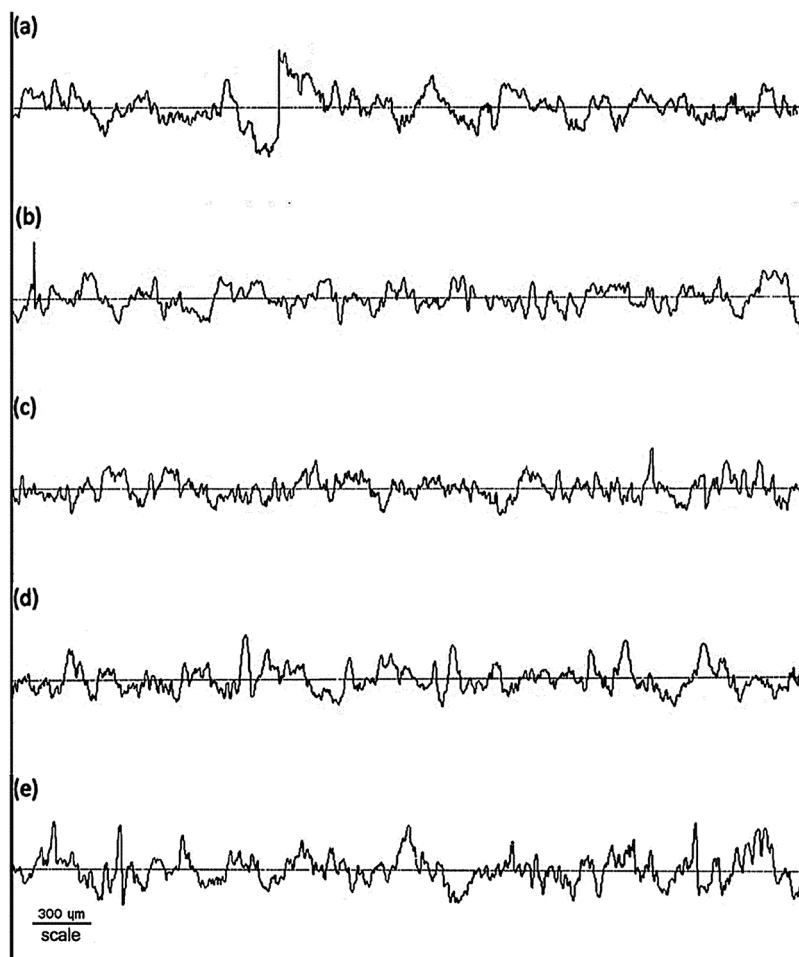


Figure 4: Surface roughness of BCNs film: (a) Non-HPH, (b) 5 cycles, (c) 10 cycles, (d) 15 cycles, and (e) 20 cycles

Table 3: The average roughness (Ra), height of average roughness (Rz), root mean square roughness (Rq), and thickness (t) of BCNs film after HPH process with various cycles

HPH Process	Ra (μm)	Rz (μm)	Rq (μm)	t (nm)
Non-HPH	1.13 ± 0.01	6.30 ± 0.32	1.38 ± 0.02	42 ± 3.7
5 Cycles	1.11 ± 0.06	6.51 ± 0.37	1.39 ± 0.09	29 ± 3.8
10 Cycles	0.93 ± 0.10	5.43 ± 0.48	1.15 ± 0.11	26 ± 4.7
15 Cycles	1.18 ± 0.20	6.37 ± 1.11	1.45 ± 0.23	25 ± 1.6
20 Cycles	1.23 ± 0.11	7.26 ± 0.91	1.55 ± 0.16	23 ± 1.8

3.5 Porosity Analysis

The effect of HPH cycle on BCNs film porosity is shown in Fig. 5. Porosity is important to transport oxygen and diffused water into BCNs film parts. BCNs film consisted of three-dimensional nanofibers generated in the surface area having high porosity [40]. The BCNs film sample without HPH process has a porosity value $62 \pm 3.9\%$. This porosity is similar to previous study that BC film from pellicle had

porosity up to 60% [41]. After 5, 10 and 15 cycles HPH process, BCNs porosity decreases to $50 \pm 1.3\%$, $42 \pm 1.3\%$, $34 \pm 2\%$ and $32 \pm 1.8\%$, respectively. A slight declined in BCNs porosity was observed after increase in HPH cycles from 15 to 20. The reducing in diameter cause the increased surface area and high density of hydroxyl groups make strongly interaction and tend to condensed. Interestingly, the number of HPH cycle controlled the porosity percentage of the formed BCNs film.

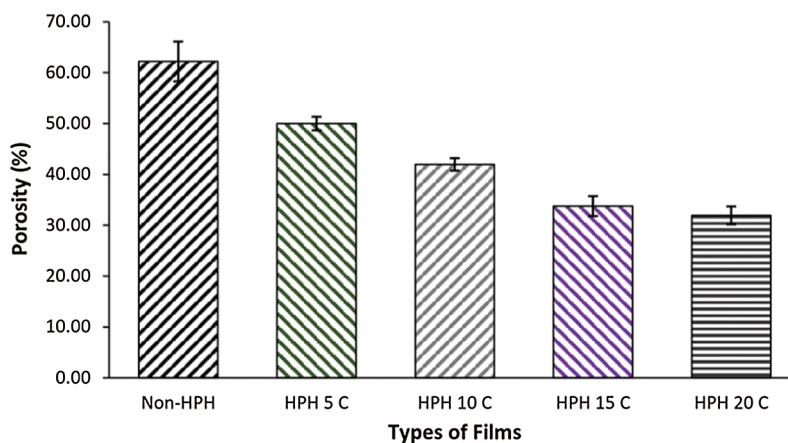


Figure 5: Porosity of BCNs film: (a) Non-HPH, (b) 5 cycles, (c) 10 cycles, (d) 15 cycles, and (e) 20 cycles

3.6 Mechanical Properties

The impact of HPH process on tensile strength and elongation of BCNs film was examined as shown in Fig. 6. The tensile strength for non-HPH sample is 68.96 ± 9.21 MPa, and after 5, 10, 15 cycles of HPH process, the tensile strength gain values 88.21 ± 22.26 , 109.15 ± 12.03 , 91.79 ± 17.27 , and 92.1 ± 21.83 MPa, with increased tensile strength by about 28.3%, 58.3%, 33.1%, and 33.6%, respectively. Fig. 6 also shows the rise in the sample elongations from $2.88 \pm 0.01\%$ in non-HPH to $2.50 \pm 0.01\%$ for 5, $3.20 \pm 0.01\%$ for 10, $3.28 \pm 0.01\%$ for 15, and 3.71 ± 0.01 for 20 cycles. These results show that HPH process with certain cycle variations could change the fiber network, the interaction between hydrogen bonds, and even entanglement. HPH cycles result in optimum inter-fiber interactions which lead to a network structure. These interactions influence the BCNs film tensile strength by strengthening or weakening the connectivity between fibrils on the BCNs film [42]. Lee et al. reported that hydroxypropyl cellulose film reinforced with cellulose fibrils after the 5–10 passes through the homogenizer improved significantly the strength strength and tensile modulus [30]. Similar with this results, the BCNs film produced through the HPH process with cycle variations affects the mechanical properties of the film and BCNs films after 10 cycles HPH process was found to be optimum.

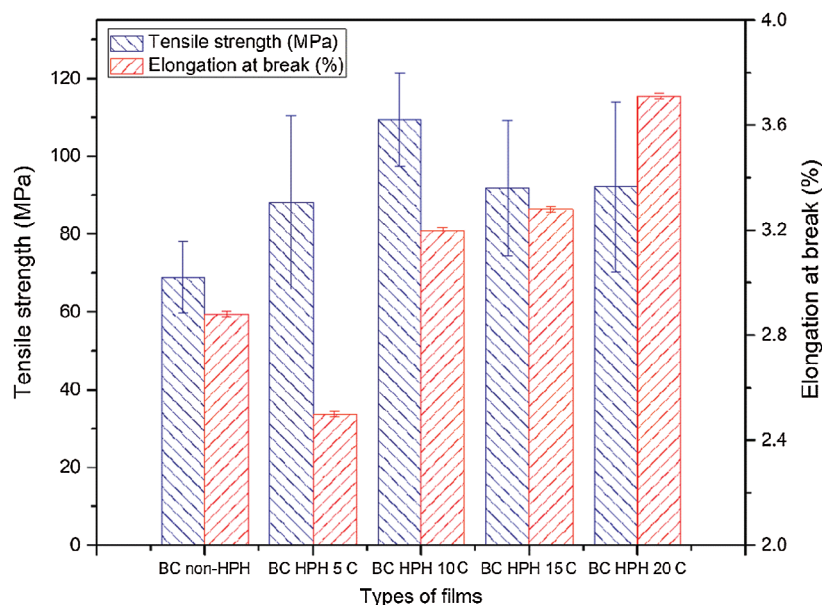


Figure 6: Mechanical properties of BCNs film: (a) Non-HPH, (b) 5 cycles, (c) 10 cycles, (d) 15 cycles, and (e) 20 cycles

4 Conclusion

The present work reports the effects of HPH cycle to BCNs film properties. After different cycles levels of homogenization process, BCNs films were prepared. After HPH treatment of 20 cycles, the fiber diameter was reduced from 61.7 nm (control) to 46.38 nm; the crystalline index decreased from 83% to 74% and, the crystallite size was found to decrease from 29.2 nm to 22.3 nm. However, the HPH cycles cause a slight reduction in the transmittance peak intensity, but, it does not affect the BCNs functional group. The implementation of HPH cycles reduces the surface roughness reduced until 10 cycles with Ra of 0.93 μm . The porosity of BCNs films was reduced after higher HPH cycles. The implementation of 10 cycles HPH to BCNs was found to be optimum with a smoother surface and maximum tensile strength of 109.15 MPa. In the future, the engineered BCNs film structure could be developed into many applications in fields packaging, food industry, medicine, cosmetics, and membranes separator in the lithium-ion battery system.

Funding Statement: Author acknowledge funding support by the Universitas Negeri Malang for the PNPB research grant for PUI CAMRY with Contract No. 4.3.714/UN32.14.1/LT/2020.

Conflicts of Interest: The authors declare that they have no conflicts of interest to report regarding the present study.

References

1. Figueiredo, A. R. P., Vilela, C., Neto, C. P., Silvestre, A. J. D., Freire, C. S. R. (2014). Bacterial cellulose-based nanocomposites: roadmap for innovative materials. In: Thakur, V. K. (ed.), pp. 17–64. *Nanocellulose polymer nanocomposites: fundamentals and applications*.
2. Lestari, P., Elfrida, N., Suryani, A., Suryadi, Y. (2014). Study on the production of bacterial cellulose from acetobacter xylinum using agro-waste. *Jordan Journal of Biological Sciences Short Communication*, 7(1), 75–80. DOI 10.12816/0008218.
3. Halib, N., Amin, M. C. I. M., Ahmad, I. (2012). Physicochemical properties and characterization of nata de coco from local food industries as a source of cellulose. *Sains Malaysiana*, 41(2), 205–211.

4. Retegi, A., Gabilondo, N., Peña, C., Zuluaga, R., Castro, C. et al. (2010). Bacterial cellulose films with controlled microstructure-mechanical property relationships. *Cellulose*, 17(3), 661–669. DOI 10.1007/s10570-009-9389-7.
5. Respati, E. (2016). Outlook of agriculture commodity on horticulture sub-sector, the center of agriculture data and information, secretary-general of ministry of agriculture of Republic Indonesia (in Indonesian), Jakarta.
6. Klemm, D., Kramer, F., Moritz, S., Lindström, T., Ankerfors, M. et al. (2011). Nanocelluloses: a new family of nature-based materials. *Angewandte Chemie International Edition*, 50(24), 5438–5466. DOI 10.1002/anie.201001273.
7. Lin, D., Li, R., Lopez-Sanchez, P., Li, Z. (2015). Physical properties of bacterial cellulose aqueous suspensions treated by high pressure homogenizer. *Food Hydrocolloids*, 44(3), 435–442. DOI 10.1016/j.foodhyd.2014.10.019.
8. Cazón, P., Velázquez, G., Vázquez, M. (2019). Characterization of bacterial cellulose films combined with chitosan and polyvinyl alcohol: evaluation of mechanical and barrier properties. *Carbohydrate Polymers*, 216, 72–85.
9. Koh, L. L. A., Chandrapala, J., Zisu, B., Martin, G. J. O., Kentish, S. E. et al. (2014). A comparison of the effectiveness of sonication, high shear mixing and homogenisation on improving the heat stability of whey protein solutions. *Food and Bioprocess Technology*, 7(2), 556–566. DOI 10.1007/s11947-013-1072-1.
10. Suryanto, H., Muhajir, M., Sutrisno, T. A., Yanuhar, U., Bintara, R. D. (2020). Effect of disintegration process on the properties of bacterial cellulose foam. *Key Engineering Materials*, 851(851), 86–91. DOI 10.4028/www.scientific.net/KEM.851.86.
11. Li, M., Cheng, Y. L., Fu, N., Li, D., Adhikari, B. et al. (2014). Isolation and characterization of corncob cellulose fibers using microwave-assisted chemical treatments. *International Journal of Food*, 10(3), 427–436.
12. Chakraborty, A., Sain, M., Kortschot, M. (2005). Cellulose microfibrils: a novel method of preparation using high shear refining and cryocrushing. *Holzforschung*, 59(1), 102–107. DOI 10.1515/HF.2005.016.
13. Jonoobi, M., Mathew, A. P., Oksman, K. (2012). Producing low-cost cellulose nanofiber from sludge as new source of raw materials. *Industrial Crops and Products*, 40(40), 232–238. DOI 10.1016/j.indcrop.2012.03.018.
14. Saelee, K., Yingkamhaeng, N., Nimchua, T., Sukyai, P. (2016). An environmentally friendly xylanase-assisted pretreatment for cellulose nanofibrils isolation from sugarcane bagasse by high-pressure homogenization. *Industrial Crops and Products*, 82, 149–160. DOI 10.1016/j.indcrop.2015.11.064.
15. Ferrer, A., Filpponen, I., Rodríguez, A., Laine, J., Rojas, O. J. (2012). Valorization of residual Empty Palm Fruit Bunch Fibers (EPFBF) by microfluidization: production of nanofibrillated cellulose and EPFBF nanopaper. *Bioresource Technology*, 125, 249–255. DOI 10.1016/j.biortech.2012.08.108.
16. Pääkko, M., Ankerfors, M., Kosonen, H., Nykänen, A., Ahola, S. et al. (2007). Enzymatic hydrolysis combined with mechanical shearing and high-pressure homogenization for nanoscale cellulose fibrils and strong gels. *Biomacromolecules*, (8), 1934–1941.
17. Kubo, M. T. K., Augusto, P. E. D., Cristianini, M. (2013). Effect of high pressure homogenization (HPH) on the physical stability of tomato juice. *Food Research International*, 51(1), 170–179. DOI 10.1016/j.foodres.2012.12.004.
18. Lenhart, V., Quodbach, J., Kleinebudde, P. (2019). Fibrillated cellulose via high pressure homogenization: analysis and application for orodispersible films. *AAPS PharmSciTech*, (21), 33.
19. Wang, Y., Wei, X., Li, J., Wang, F., Wang, Q. et al. (2015). Study on nanocellulose by high pressure homogenization in homogeneous isolation. *Fibers and Polymers*, 16(3), 572–578. DOI 10.1007/s12221-015-0572-1.
20. Donsí, F., Wang, Y., Li, J. I., Huang, Q. (2010). Preparation of curcumin sub-micrometer dispersions by high-pressure homogenization. *Journal of Agricultural and Food Chemistry*, (58), 2848–2853.
21. Mautner, A. (2020). Nanocellulose water treatment membranes and filters: a review. *Polymer International*, 69(9), 741–751. DOI 10.1002/pi.5993.
22. Kawee, N., Lam, N. T., Sukyai, P. (2018). Homogenous isolation of individualized bacterial nanofibrillated cellulose by high pressure homogenization. *Carbohydrate Polymers*, 179(4), 394–401. DOI 10.1016/j.carbpol.2017.09.101.
23. Liu, Y. (2012). Homogeneous isolation of nanocellulose from sugarcane bagasse by high pressure homogenization. *Carbohydrate Polymers*, 90(4), 1609–1613. DOI 10.1016/j.carbpol.2012.07.038.

24. Hongrattanavichit, I., Aht-ong, D. (2020). Nanofibrillation and characterization of sugarcane bagasse agro-waste using water-based steam explosion and high-pressure homogenization. *Journal of Cleaner Production*, 277(5), 123471. DOI 10.1016/j.jclepro.2020.123471.
25. Ang, S., Haritos, V., Batchelor, W. (2019). Effect of refining and homogenization on nanocellulose fiber development, sheet strength and energy consumption. *Cellulose*, 26(8), 4767–4786. DOI 10.1007/s10570-019-02400-5.
26. Suryanto, H., Marsyahyo, E., Irawan, Y. S., Soenoko, R. (2013). Effect of alkali treatment on crystalline structure of cellulose fiber from mendong (*fimbristylis globulosa*) straw. *Key Engineering Materials*, 594–595, 720–724. DOI 10.4028/www.scientific.net/KEM.594-595.720.
27. Suryanto, H., Jenuardy, S., Kustono, D., Puspitasari, P., Lubis, D. Z. (2018). Sonication assisted synthesis of biocomposite from starch/nanoclay and its properties. *International Review of Mechanical Engineering*, (12), 272–278.
28. Hassan, E., Hassan, M., Abou-zeid, R., Berglund, L., Oksman, K. (2017). Use of bacterial cellulose and crosslinked cellulose nanofibers membranes for removal of oil from oil-in-water emulsions. *Polymers*, 9(12), 388. DOI 10.3390/polym9090388.
29. Ren, S., Sun, X., Lei, T., Wu, Q. (2014). The effect of chemical and high-pressure homogenization treatment conditions on the morphology of cellulose nanoparticles. *Journal of Nanomaterials*, 2014(18), 1–11. DOI 10.1155/2014/582913.
30. Lee, S. Y., Chun, S. J. (2009). Preparation of cellulose nanofibrils by high-pressure homogenizer and cellulose-based composite films. *Journal of Industrial and Engineering Chemistry*, 15(15), 50–55. DOI 10.1016/j.jiec.2008.07.008.
31. Vicente, A. T., Araújo, A., Gaspar, D., Santos, L., Marques, A. C. et al. (2017). Optoelectronics and bio devices on paper powered by solar cells. In: Das, N. (ed.), *Nanostructured solar cells*. London: IntechOpen.
32. Mem, C. K., Ting, S. S., Lin, O. H. (2019). Comparative properties analysis between microcrystalline cellulose and cellulose nanocrystals extracted from rice straw. *Malaysian Journal of Microscopy*, (15), 146–154.
33. Galiwango, E., Abdel, N. S., Al-marzouqi, A. H., Abu-omar, M. M., Khaleel, A. A. (2019). Isolation and characterization of cellulose and α -cellulose from date palm biomass waste. *Heliyon*, 5(12), e02937. DOI 10.1016/j.heliyon.2019.e02937.
34. Li, J., Wei, X., Wang, Q., Chen, J., Chang, G. et al. (2012). Homogeneous isolation of nanocellulose from sugarcane bagasse by high pressure homogenization. *Carbohydrate Polymers*, 90(4), 1609–1613. DOI 10.1016/j.carbpol.2012.07.038.
35. Abol-fotouh, D., Hassan, M. A., Shokry, H., Roig, A., Azab, M. S. et al. (2020). Bacterial nanocellulose from agro-industrial wastes: low-cost and enhanced production by *Komagataeibacter saccharivorans*. *Scientific Reports*, (10), 1–14.
36. Eyholzer, C., Bordeanu, N., Lopez-Suevos, F., Rentsch, D., Zimmermann, T. et al. (2010). Preparation and characterization of water-redispersible nanofibrillated cellulose in powder form. *Cellulose*, 17(1), 19–30. DOI 10.1007/s10570-009-9372-3.
37. Abrial, H., Lawrensius, V., Handayani, D., Sugiarti, E. (2018). Preparation of nano-sized particles from bacterial cellulose using ultrasonication and their characterization. *Carbohydrate Polymers*, 191(2), 161–167. DOI 10.1016/j.carbpol.2018.03.026.
38. Han, J., Zhou, C., Wu, Y., Liu, F., Wu, Q. (2013). Self-assembling behavior of cellulose nanoparticles during freeze-drying: effect of suspension concentration, particle size, crystal structure, and surface charge. *Biomacromolecules*, 14(5), 1529–1540. DOI 10.1021/bm4001734.
39. Pogorelova, N., Rogachev, E., Digel, I., Chernigova, S., Nardin, D. (2020). Bacterial cellulose nanocomposites: morphology and mechanical properties. *Materials*, 13(12), 2849–2816. DOI 10.3390/ma13122849.
40. Esa, F., Tasirin, S. M., Rahman, N. A. (2014). Overview of bacterial cellulose production and application. *Agriculture and Agricultural Science Procedia*, 2(2), 113–119. DOI 10.1016/j.aaspro.2014.11.017.
41. Wang, S. S., Han, Y. H., Chen, J. L., Zhang, D. C., Shi, X. X. et al. (2018). Insights into bacterial cellulose biosynthesis from different carbon sources and the associated biochemical transformation pathways in *Komagataeibacter* sp. W1. *Polymers*, (10), 1–20.
42. Dayal, M. S., Catchmark, J. M. (2016). Mechanical and structural property analysis of bacterial cellulose composites. *Carbohydrate Polymers*, 144(2), 447–453. DOI 10.1016/j.carbpol.2016.02.055.